AGU ADVANCING EARTH AND SPACE SCIENCE

Water Resources Research

RESEARCH ARTICLE
10.1029/2019WR026252

Emergent Hydrodynamics and Skimming Flow Over Mussel Covered Beds in Rivers

B. J. Sansom[1], S. J. Bennett[2], J. F. Atkinson[1], and C. C. Vaughn[3]

[1]Department of Civil, Structural, and Environmental Engineering, SUNY University at Buffalo, Buffalo, NY, USA, [2]Department of Geography, SUNY University at Buffalo, Buffalo, NY, USA, [3]Oklahoma Biological Survey and Department of Biology, University of Oklahoma, Norman, OK, USA

Key Points:

- Partially exposed mussels disrupt the distribution and magnitudes of longitudinal flow velocity and Reynolds shear stress depending on mussel density
- Above densities of 25 mussels m^{-2}, a hydrodynamic transition occurs that reduces longitudinal flow velocity and turbulent shear stress near the bed
- Mussel-induced skimming flow decreases the dislodgment potential and thereby enhances bed stability and the long-term persistence of mussels

Correspondence to:
B. J. Sansom,
bsansom@buffalo.edu

Citation:
Sansom, B. J., Bennett, S. J., Atkinson, J. F., & Vaughn, C. C. (2020). Emergent hydrodynamics and skimming flow over mussel covered beds in rivers. *Water Resources Research*, *56*, e2019WR026252. https://doi.org/10.1029/2019WR026252

Received 3 SEP 2019
Accepted 15 JUN 2020
Accepted article online 19 June 2020

Abstract Freshwater mussels are dominant ecosystem engineers in many streams throughout North America, yet they remain among the world's most imperiled fauna. Extensive research has quantified the ecological role of mussels in aquatic habitats, but little is known about the interaction between mussels and their surrounding physical and hydrodynamic habitat. Here the physical interactions of mussels with near-bed flow are investigated in an experimental channel using model mussels. The results show that (1) mussels disrupt the distributions and magnitudes of time-averaged values of longitudinal flow velocity and Reynolds shear stress depending on mussel density, and (2) at densities of approximately 25 mussels m^{-2} and greater, a hydrodynamic transition occurs where the maximum Reynolds shear stress is displaced from the bed to the height of the mussel canopy, near-bed longitudinal flow velocity is reduced, and average turbulent shear stresses acting on the mussels are reduced by as much as 64%, thus markedly decreasing the dislodgement potential of the mussels by these stresses. These results provide strong empirical evidence for a positive density-dependent effect related to flow-organism interactions and their ecological success, such as enhancing river bed hydrodynamic habitat complexity or decreasing the turbulent shear stresses acting to dislodge mussels from the river bed. This information will improve the understanding of the long-term persistence of mussel beds and help focus future conservation strategies.

Plain Language Summary Freshwater mussels are important aquatic organisms that contribute to the structure and function of aquatic ecosystems. Yet mussels are globally threatened, and it is not understood how mussels have adapted to persist in chronically unstable environments such as rivers. Here we show that the protrusion of mussels into the water column modifies near-bed turbulent flow. At mussel densities greater than 25 mussels m^{-2}, a hydrodynamic phenomenon emerges where two distinct flow layers are present. In the inner flow, the area from the river bed to the height of the protruded mussels, longitudinal flow velocity and turbulent shear stresses are greatly reduced and the maximum shear stress is displaced off the river bed to the height of the protruded mussels. In the outer flow, the area from the height of the protruded mussels to the water surface, longitudinal flow velocity increases but the maximum turbulent shear stress remains constant. The ability of mussels to modify the hydrodynamic habitat of rivers has important ecological and conservation implications, such as enhancing river bed habitat complexity or decreasing the turbulent shear stresses acting to dislodge mussels from the river bed. This information is necessary to improve future conservation and management strategies for freshwater mussels.

1. Introduction

Aquatic ecosystems are largely controlled by the interplay between biological, physical, and chemical processes at multiple scales (Nikora, 2010; Statzner et al., 1988). Among these processes, organism interactions with flow can exert strong effects on hydrodynamics, which thereby affect the form, function, and dynamics of fluvial systems (Allen et al., 2014; Nikora, 2010). For example, aquatic vegetation alters turbulent flow, increases flow resistance, and reduces sediment conveyance (Jones et al., 2012; Nepf & Vivoni, 2000), and net-spinning caddisflies (*Hydropsyche* spp.) increase the stability of benthic substrate and food availability while providing localized refugia for other species (Cardinale et al., 2004; Nakano et al., 2005). These organisms are often classified as ecosystem engineers since they can change the availability of resources to other species through physical modifications of biotic or abiotic components (Jones et al., 1994).

Freshwater mussels (Bivalvia: Unionida) are also ecosystem engineers that play important roles in structuring aquatic ecosystems. In North America, mussels occur as dominant benthic invertebrates; they can account for 50% to 90% of the benthic biomass, and densities (number of mussels per m^2) on some river beds can exceed 100 mussels m^{-2} (Allen & Vaughn, 2010; Strayer et al., 1994). As filter feeders, they excrete nutrients that stimulate primary and secondary production (Atkinson et al., 2013; Spooner et al., 2012) and their burrowing activity modifies nutrient distribution in the sediments and provides niche partitioning between mussel species (Allen & Vaughn, 2009; Lohrer et al., 2004). Burrowed mussel shells often protrude a few centimeters into the water column and provide substrate for epibiont attachment, refuge for benthic organisms, and contribute to habitat complexity (Allen & Vaughn, 2009; Gutiérrez et al., 2003; Hopper et al., 2019).

Once ubiquitous in rivers, mussels now are a globally imperiled fauna primarily due to habitat destruction and degradation, overharvest, and invasive species (Haag, 2012; Strayer, 2008). In rivers, mussels often occur as dense, multispecies assemblages called mussel beds that are patchily distributed and separated by areas where mussels do not occur or are sparse (Atkinson & Vaughn, 2015; Strayer, 2008). As a basis to understand habitat and conservation approaches, it has been suggested that mussel beds occur in flow refugia patches on river beds where shear stresses during floods with moderately long return periods (from 3 to 30 years) are too low to displace or entrain the organisms or the sediments in which they are found (Strayer, 1999). But many mussel assemblages can persist at a given river reach for multiple decades (20 to more than 100 years) and withstand repeated channel-forming discharges with no adverse effect on mussel density or assemblage composition (Sansom, Bennett, et al., 2018). These observations suggest that the flow refugia hypothesis alone is not sufficient to explain mussel occurrence and that additional factors are important in promoting mussel survival.

A clear understanding of the relationship between mussels and their physical and hydrodynamic habitat has yet to be resolved. Numerous studies have attempted to explain mussel occurrence by correlating mussel abundance or distribution to hydraulic variables or through using computer simulations or predictive statistical models. Ultimately, field studies have had limited success (Hardison & Layzer, 2001; Layzer & Madison, 1995) or are often conducted during low flows where hydraulic variables are likely not a limiting factor to mussel occurrence (Hardison & Layzer, 2001). Other approaches estimate hydraulic variables at high flows using channel geomorphology rather than direct measurements (Gangloff & Feminella, 2006; Howard & Cuffey, 2003) or rely on models with assumptions that have not been adequately tested in the field (Morales et al., 2006a, 2006b) and do not examine direct interactions between mussels and hydraulic or physical variables. Moreover, an alternative explanation to the flow refugia hypothesis is that mussels themselves increase bed stability through biophysical interactions with hydraulic and physical variables (Johnson & Brown, 2000; Strayer, 2008; Zimmerman & de Szalay, 2007), but this idea has not been rigorously tested in freshwater systems across multiple scales.

The few studies that have quantified the interaction between mussels and hydrodynamics have either focused on marine tidal environments or have been limited to the scale of a single mussel or a small group of mussels for freshwater systems. Annular flume studies representing marine tidal environments with dense assemblages of mussels (55% and 95% bed coverage) demonstrated that mussels increase sediment erosion due to higher near-bed turbulence and shear stress relative to bare sediment (Widdows et al., 2009). The suspension feeding of marine bivalves can enhance the feeding efficiency of individual mussels within a mussel bed and affect the development of boundary layer flow (Monismith et al., 1990; O'Riordan et al., 1993; Widdows et al., 2009). For freshwater systems, experimental studies have examined flow around a single mussel, demonstrating that nonfiltering and filtering mussels increase turbulent kinetic energy, with a greater increase for filtering mussels (Kumar et al., 2019; Sansom, Atkinson, et al., 2018). Moreover, computational fluid dynamic modeling of flow around a small cluster of nonfiltering mussels showed that exposed mussel shells induce a complex turbulent flow field that may increase sediment entrainment around and downstream of the mussels (Constantinescu et al., 2013). While these studies illustrate important mussel-flow interactions, there remains a need to investigate mussel-flow interactions beyond an individual mussel scale in freshwater systems and how these interactions contribute to mussel survival and to the form and function of rivers.

In a partially buried position, mussel shells protrude into the water column and represent roughness elements on the streambed. The spacing, density, and height of exposure of roughness elements can

influence the type of near-bed flow and hydrodynamic habitat that occurs over a rough surface (Chow, 1959). For context, three distinct flow regimes have been identified for pipe flow over transverse roughness elements (Morris, 1955): (1) isolated roughness flow, in which the roughness elements are spaced relatively far apart with little interaction, (2) wake-interference flow, in which the roughness elements are sufficiently close together so that the wake zones for individual elements interact with downstream elements, and (3) skimming flow, in which the roughness elements are so closely spaced that the outer flow essentially skims over the crests of the elements (Knight & Macdonald, 1979; Perry et al., 1969). Each flow regime results in differing hydrodynamic characteristics (Allan & Castillo, 2007; Wolfe & Nickling, 1993). Flow around isolated roughness elements produces horseshoe vortices that create several unique hydrodynamic microhabitats (Constantinescu et al., 2013; Davis, 1986). In wake interference flow, the partitioning of these microhabitats breaks down. In skimming flow, the hydrodynamic habitat is characterized by a layer of high longitudinal velocity near the top of the roughness element and a layer of reduced longitudinal velocity in the interstices between the roughness elements (Davis & Barmuta, 1989). Yet these previous studies have been limited to examining flow around isolated roughness elements (Constantinescu et al., 2013; Kumar et al., 2019; Sansom, Atkinson, et al., 2018). The full extent of flow modification across an entire mussel bed at varying mussel densities, mussel species, and flow regimes remains unknown.

The objectives of this study were to investigate how the presence of freshwater mussels modulates near-bed flow and turbulent shear stresses. Experiments were conducted across a range of mussel densities in an experimental channel using model mussels to mimic shell roughness and two-dimensional particle image velocimetry to characterize the turbulent flow.

2. Materials and Methods

Experiments were performed in a recirculating hydraulic flume 10.7 m long and 0.47 m wide. The flume was fitted with bed inserts constructed of lumber and plywood sheets. Gravel ($D_{50} = 0.01$ m) was affixed to the plywood sheet to resemble a gravel streambed (Figure 1). Model mussels were constructed from red oak wooden blocks to simulate a river bed covered by partially exposed mussels. Model mussels were designed using a 3-D scan of a *Lampsilis siliquoidea* shell, a common smooth-shelled mussel species found throughout western New York and elsewhere in the United States and Canada with a similar morphology to other common species (Parmalee & Bogan, 1998). Model mussels were constructed and placed on top of the bed inserts to simulate the posterior end of a partially exposed mussel in a burrowed state (Figure 1). In this position, *L. siliquoidea* has an average length of shell exposure in river beds of ~3 to 4 cm (Sansom, 2018). Model mussels also included a 6 mm diameter hole near the distal end to represent the excurrent aperture; a companion study examined the effects of filter feeding on near-bed flow (see Sansom, 2018).

The protrusion height of the model mussels was maintained at 3.5 cm, and all mussels were aligned parallel to the flow (Figure 1). Experiments were conducted at 10 different mussel densities, ranging from 0 to 100 mussels m^{-2}, which represent a range of natural mussel densities (Allen & Vaughn, 2010; Sansom, Bennett, et al., 2018). The test with no mussels served as a control. The spatial distribution of shells at the highest mussel density of 100 mussels m^{-2} was determined using a random number generator to assign each mussel a unique spatial position (longitudinal x and cross-stream y) in the flume. Lower mussel densities were obtained using a random number generator to select mussels for removal until the target density was achieved.

Flow measurements were made for each mussel density using a constant water depth d of 0.15 m and four target Froude Fr numbers: 0.12, 0.25, 0.37, and 0.50, defined as $Fr = \overline{U}/\sqrt{gd}$ where $\overline{U}$ is depth-averaged longitudinal velocity and g is gravitational acceleration. The mean corresponding $\overline{U}$ ($\pm$ standard error, SE) across all mussel densities for each target Fr was 0.13 $\pm$ 0.003, 0.26 $\pm$ 0.005, 0.38 $\pm$ 0.005, and 0.52 $\pm$ 0.007 m s^{-1}, respectively (see Appendix 1). These Fr numbers correspond to natural flows ranging from baseflow to bank-full conditions for two streams with ecologically and historically important mussel populations (Sansom, Bennett, et al., 2018).

At each density and target Fr number, particle image velocimetry (PIV) was used to measure the two-dimensional velocities along the centerline of the flume at a single location 5.5 m downstream of the leading edge of the mussel bed (Figure 1). The flow was seeded with hollow glass spheres 13 μm in

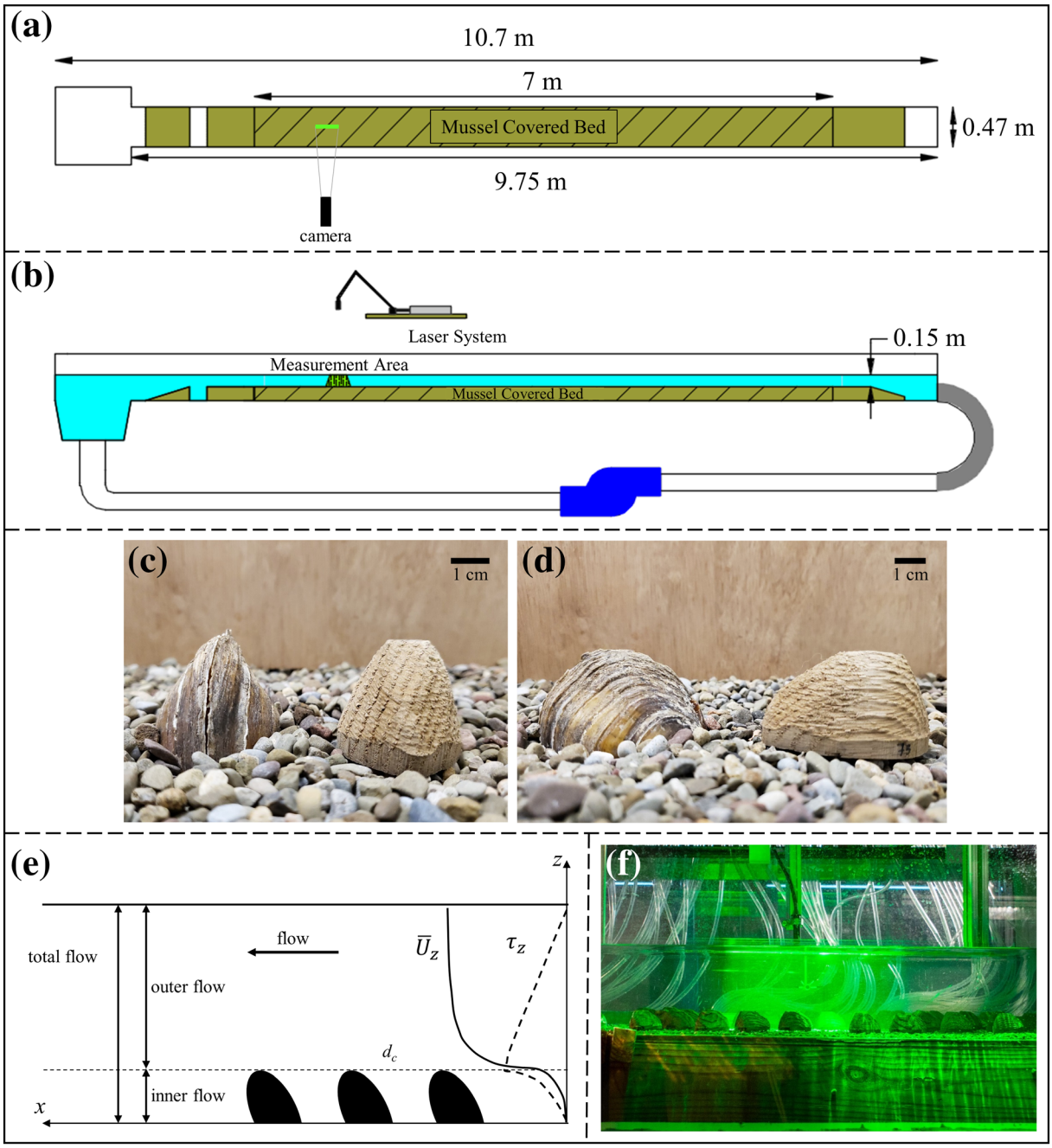

Figure 1. Conceptual diagram of experimental campaign. Experiments were conducted with a modeled mussel bed with mussel densities ranging from 0 to 100 mussels m^{-2} fitted in a recirculating flume (plan view (a) and side view (b)). The green line in panel (a) and the green-dashed region in panel (b) represent the PIV field of view 5.5 downstream the leading edge of the mussel bed and along the center line of the flume. The model mussels were constructed with wooden blocks using a 3-D scan of a mussel shell partially exposed in the water column. (c and d) The front and side views, respectively, for the partially buried mussel shell (left) and model mussel (right). (e) The three flow regions, along with hypothesized time- and space-averaged profiles for velocity $\overline{U}_z$ and Reynolds shear stress τ_z in the presence of skimming flow. Velocity was measured in the designated measurement area (b) with particle image velocimetry (PIV), and all model mussels protruded 3.5 cm into the flow and were aligned parallel with the flow (f). Flow is from right to left in all panels.

diameter (Potters Industries Inc., SH400S20, Carlstadt, New Jersey) and illuminated with a laser-sheet generated by a 50 mJ Nd:YAG pulsed laser system (Litron Lasers, LM0441, Ruby, England). The PIV field of view extended 0.27 m along the longitudinal direction x_{bed} and the entire flow depth d. To provide a stable laser plane and allow the laser light sheet to penetrate through the water column unimpeded, a

3 cm wide, 5 mm thick, and 60 cm long polycarbonate window was suspended above the flume that just touched the free water surface. This window caused a reduction in the near-surface longitudinal velocities, which were removed from the analysis. A velocity-defect flow depth δ was defined as the distance from the bed to the height of the maximum flow velocity ($\delta \approx 0.86d$). Instantaneous velocity fields were obtained by collecting continuous PIV measurements with a 10-bit high-resolution SpeedSense 1040 camera with a resolution of 2320 × 1726 pixels (Dantec Dynamics Inc., Holtsville, NY) for 60 s at 85 Hz. Prior to the experiments, preliminary data were collected at all target *Fr* numbers to ensure that the exposure time for the camera (5,184 μs) and time between the laser pulses (860 μs) were set so that the illuminated particles moved no more than 25% of the interrogation area, set at 32 × 32 pixels. An adaptive PIV method was performed on all collected image pairs using a 32 × 32 pixel grid (3.75 mm × 3.75 mm) to quantify instantaneous velocities in longitudinal x and vertical z planes.

Acoustic Doppler velocimetry (ADV) measurements were also recorded to corroborate the PIV measurements. After the PIV data were collected for each mussel density and target *Fr* number, the polycarbonate window was removed and the ADV was positioned along the centerline of the flume and in the center of the PIV field of view (~5.64 m downstream the leading edge of the mussel bed). Unlike PIV, the ADV measures three-component velocities at a single point in the flow. Therefore, for each density and target *Fr* number, nine measurement locations were selected spanning distances of 0.01 to 0.13 m above the bed. Similar to PIV, instantaneous velocities were measured with the ADV for 60 s at 85 Hz. Velocity data from the ADV were processed by despiking anomalous observations using a phase space threshold (Goring & Nikora, 2002) and time averaged. Velocities in the longitudinal direction (i.e., u component) were compared between ADV time-averaged point data and PIV time-averaged and horizontally averaged (see below) data to verify the PIV system.

Velocity measurements from the PIV data for the longitudinal u and vertical w components were processed to determine their time-averaged values at a point (denoted by an overbar), defined as $\overline{u}$ and $\overline{w}$, respectively. These time-averaged values were used to determine the fluctuating velocity components (denoted by an accent) and Reynolds shear stress τ_{uw}, defined as follows:

$$u' = u - \overline{u}; \qquad w' = w - \overline{w}; \qquad \tau_{uw} = -\rho\overline{u'w'} \tag{1}$$

where ρ is water density (kg m^{-3}). Longitudinal velocities $\overline{U}_z$ and Reynolds shear stresses τ_z also were spatially averaged across the entire field of view at a height z above the bed (see Figure 2), defined as follows:

$$\overline{U}_z = \frac{1}{x_{bed}}\int_{x=0}^{x_{bed}} \overline{u}dx; \qquad \tau_z = \frac{1}{x_{bed}}\int_{x=0}^{x_{bed}} \tau_{uw}dx \tag{2}$$

Depth-averaged longitudinal velocities also were determined for discrete flow zones: (1) the total flow depth $\overline{U}$, defined from the top of the gravel bed ($z = 0$) inserts to the height of the maximum velocity δ, (2) the outer flow $\overline{U}_O$, defined from the top of the mussels $d_c = z/\delta = 0.27$ to δ, and (3) the inner flow $\overline{U}_I$, defined from the gravel bed to the top of the mussels d_c (Figure 1), given by

$$\overline{U} = \frac{1}{\delta}\int_{z=0}^{\delta} \overline{U}_z dz; \qquad \overline{U}_O = \frac{1}{\delta - d_c}\int_{z=d_c}^{\delta} \overline{U}_z dz; \qquad \overline{U}_I = \frac{1}{d_c}\int_{z=0}^{d_c} \overline{U}_z dz \tag{3}$$

For the no-mussel control experiments, shear velocity and the equivalent near-bed Reynolds shear stress was determined using two methods. The first method used the Kármán-Prandtl "law of the wall" applied to the lower portion (~20%) of the velocity profile (von Karman, 1931):

$$\frac{\overline{U}_z}{u_{*w}} = \frac{1}{\kappa}\ln\frac{z}{z_o}; \qquad \tau_w = \rho u_{*w}^2 \tag{4}$$

where κ is the von Kármán coefficient (0.41), z_o is the zero-velocity roughness height, and u_{*w} and τ_w are near-bed shear velocity and shear stress, respectively. The second method determined shear velocity by using the maximum value τ_{max} of the time-averaged and longitudinally averaged vertical profile of τ_z:

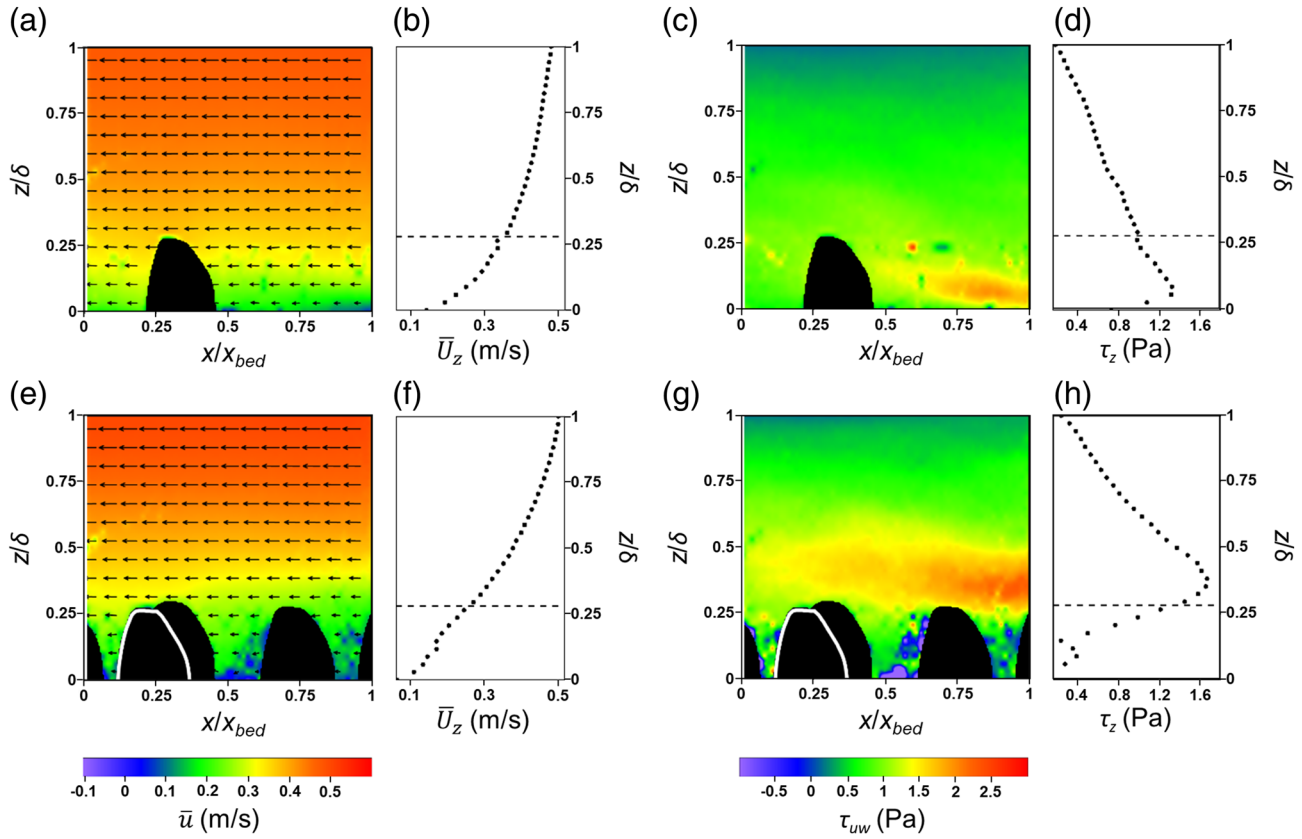

Figure 2. Example time-averaged contour plots and time-averaged and horizontally averaged vertical profiles. Time-averaged contour plots of longitudinal velocity $\overline{u}$ (a, e) and Reynolds shear stress τ_{uw} (c, g), and time-averaged and horizontally averaged velocity $\overline{U}_z$ (b, f) and Reynolds shear stress τ_z (d, h) for two example experiments, 10 mussels m^{-2}; $Fr = 0.37$ (top panel) and 100 mussels m^{-2}; $Fr = 0.37$ (bottom panel; the white outline demarcates two individual mussels). The gray dashed line in the vertical profile panels represents the height of the mussel canopy. Notice the disruption of the boundary layer flow below the height of the mussel canopy top in the 100 mussel m^{-2} experiment.

$$u_{*\tau} = \sqrt{\frac{\tau_{max}}{\rho}} \tag{5}$$

Because $u_{*w} \approx u_{*\tau}$ and $\tau_w \approx \tau_{max}$ across all target Fr numbers for the no-mussel control experiments (see Results below) and due to deviations in the logarithmic velocity profile once mussels were added to the bed inserts, shear velocity was determined using Equation 5 for all remaining experiments (Ghisalberti & Nepf, 2008; Murphy et al., 2007). To explore near-bed flow, the average turbulent shear stress acting on the mussels τ_{mussel} was defined as follows:

$$\tau_{mussel} = \frac{1}{d_c}\int_{z=0}^{d_c} \tau_z dz \tag{6}$$

Finally, we used roughness spacing S, percent bed coverage, and roughness density to empirically demonstrate the point at which mussel density causes shifts in the hydraulic flow regime. Roughness spacing S was quantified as the mean distance between successive mussels for each density. Using the ratio between roughness spacing S and the height of the roughness elements d_c, as well as the percent bed coverage, we determined the approximate flow regime (i.e., isolated roughness or skimming flow) likely present at each mussel density (Knight & Macdonald, 1979; Leonardi et al., 2007; Wolfe & Nickling, 1993). We also quantified the shift from a sparse to dense mussel canopy using a nondimensional measure of roughness density λ that represents the frontal area per bed area (Nepf, 2012; Wooding et al., 1973), defined as follows:

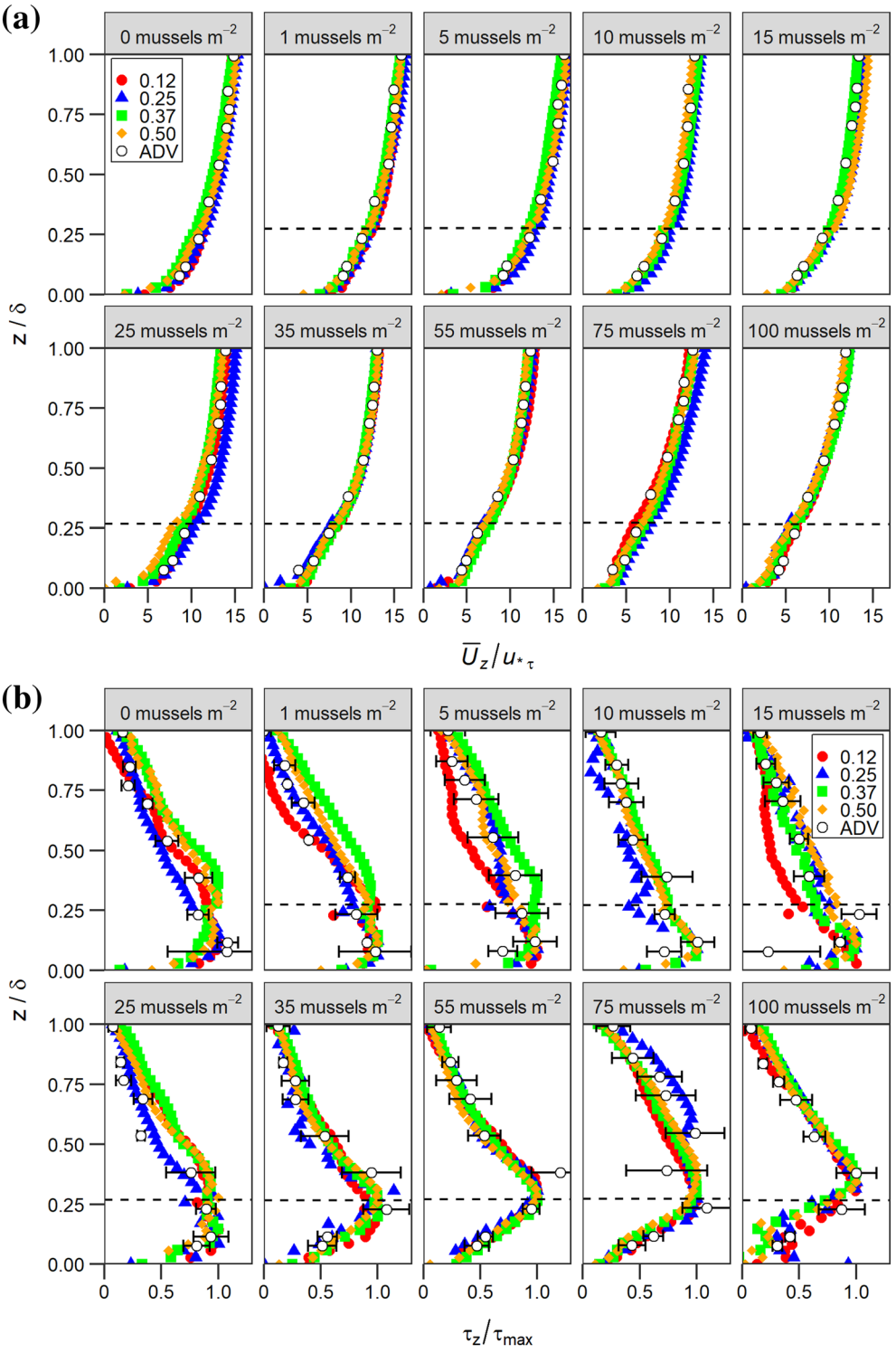

Figure 3. Normalized velocity and Reynolds shear stress profiles. Vertical profiles of normalized (a) depth-averaged velocity and (b) Reynolds shear stress for particle image velocimetry (PIV) and acoustic Doppler velocimetry (ADV) data at each mussel density. PIV data are shown for each target *Fr* number. ADV data and the associated error bars represent the mean and ±1 SE, respectively, across each target *Fr* number. In panel a, the error bars are smaller than the size of symbols used. The gray dashed line represents the height of the mussel canopy. Data were excluded for the 10 mussels m^{-2}, $Fr = 0.12$ experiment due to erroneous experimental data.

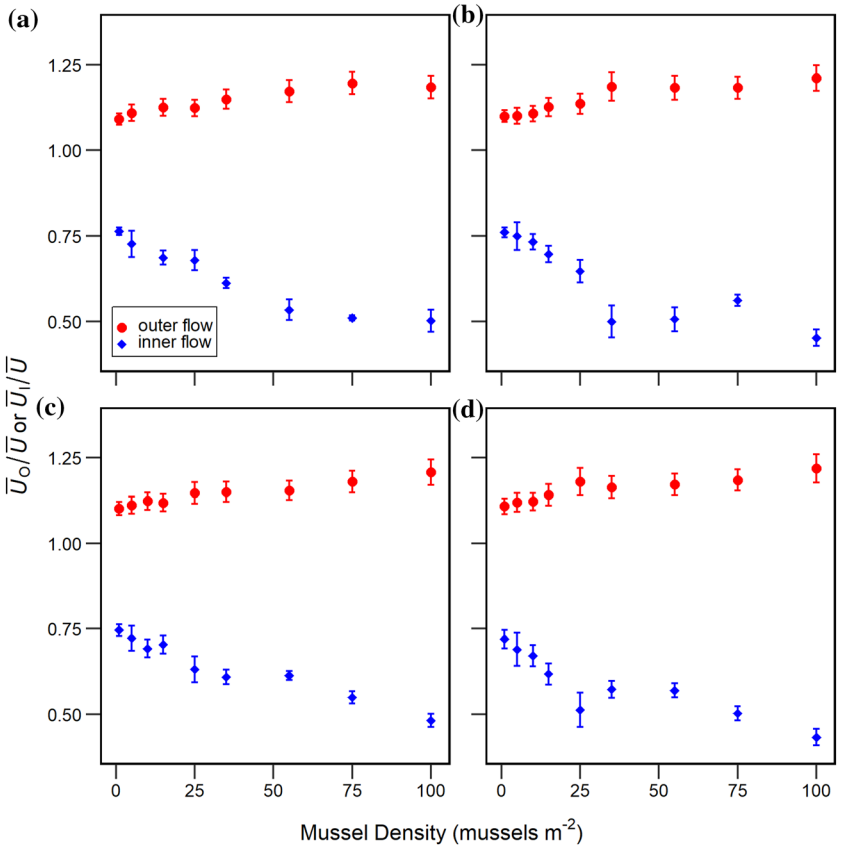

Figure 4. Normalized velocity for the inner and outer flow regions. Normalized velocity for the inner $\overline{U}_I$ and outer $\overline{U}_O$ flow regions for each flow velocity for target *Fr* numbers of (a) 0.12, (b) 0.25, (c) 0.37, and (d) 0.50 as a function of mussel density. Error bars represent ±1 S.E. of the respective normalized velocity. Data were excluded for the 10 mussels m^{-2}, $Fr = 0.12$ experiment due to erroneous experimental data.

$$\lambda = \int_{z=0}^{d_c} a dz = a d_c \tag{7}$$

where the frontal area per volume is $a = m_w/S^2$ and m_w is the midheight width of the mussel (i.e., 2.5 cm for the present tests).

3. Results

To demonstrate the spatial and time-averaged impacts of mussels on near-bed flow, Figure 2 shows example contour plots and vertical profiles of longitudinal velocity and Reynolds shear stress using PIV data. Only a single *Fr* number ($Fr = 0.37$) and two mussel densities (10 and 100 mussels m^{-2}) are shown to illustrate differences in velocity and Reynolds shear stress distributions due to mussel density. There was strong agreement in the time-averaged velocity data and Reynolds shear stress between the ADV and PIV (Figure 3). Minor differences, especially near the bed, are attributed to the PIV averaging data across the entire 0.27 m field of view, whereas the ADV data were collected and averaged at points in a single profile. As mussel density changed, the ADV data become affected by the probe's proximity to the isolated roughness elements and by the wake interference created. In Figure 3, ADV data were excluded for the following samples where the signal to noise ratio or correlation were relatively low (signal to noise ratio < 15, correlation < 70): 1 mussel m^{-2}, $Fr = 0.12$ all points, 1 mussel m^{-2}, $Fr = 0.25$ all points, and 5 mussels m^{-2}, $Fr = 0.12$ y = 3 cm sample.

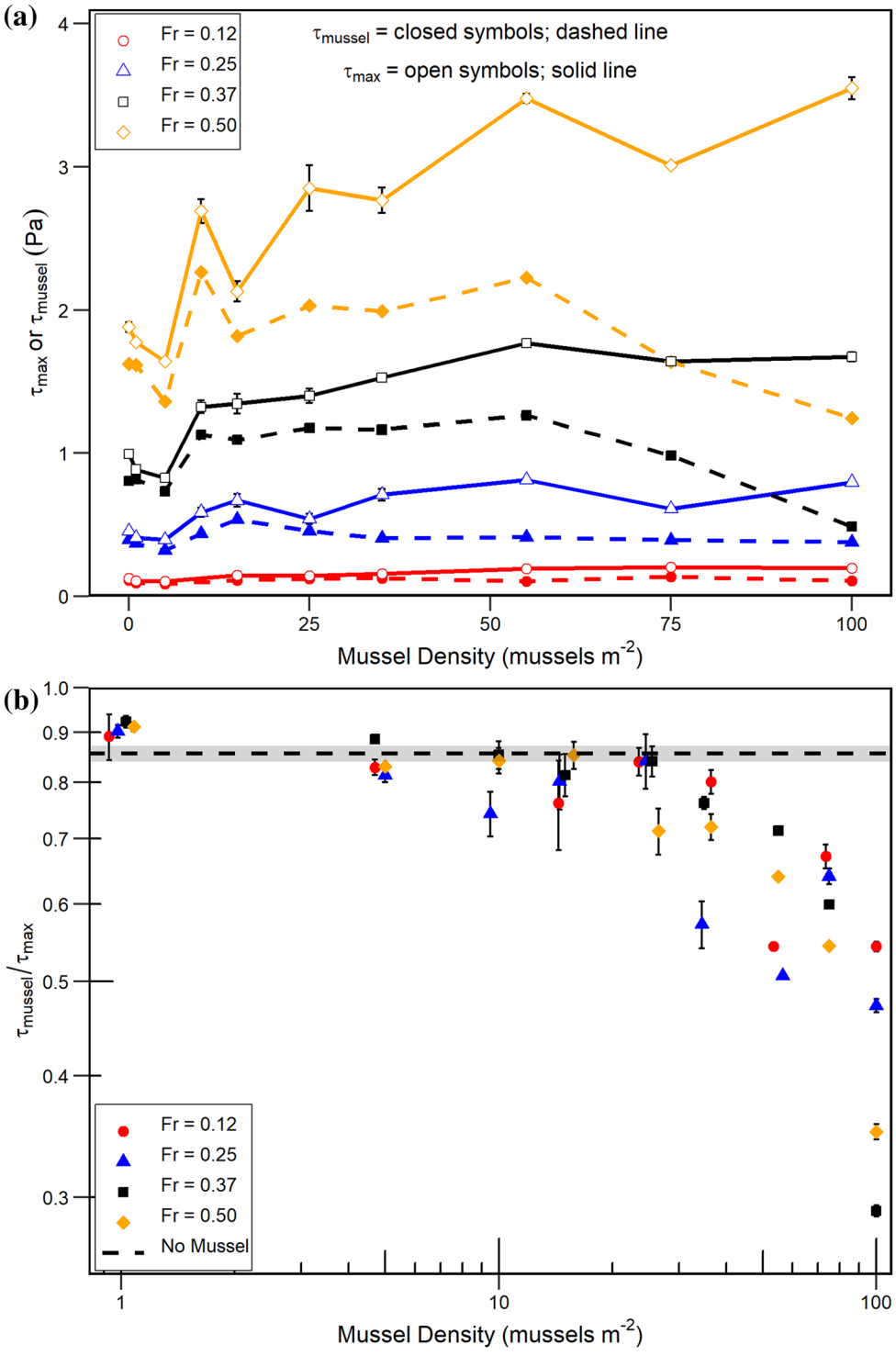

Figure 5. Variation in turbulent shear stress as a function of increasing mussel density. (a) Variation of shear stress determined using Equation 6 for τ_{mussel} or the maximum value τ_{max} of the time-averaged and longitudinally averaged vertical profile of τ_z. The error bars represent ±1 S.E. calculated from the respective Reynolds stress determination. (If error bars are not visible, they are displayed but are smaller than the size of symbols used.) (b) The ratio of the average turbulent shear stress acting on the mussels τ_{mussel} to the maximum shear stress τ_{max} decreases as mussel density increases across all target *Fr* numbers. Both axes have been log scaled, error bars represent ±1 S.E. associated with the ratio of τ_{mussel} to τ_{max} (if error bars are not visible, they are displayed but are smaller than the size of symbols used), and the shaded region represents ±1 S.E. associated with the no mussel control mean. Both panels excluded data for the 10 mussels m^{-2}, $Fr = 0.12$ due to erroneous experimental data.

Table 1
Mussel Density and Corresponding Roughness Indices: The Percent of Bed Coverage; the Mean Spacing Between Roughness Elements S, the Ratio of S to Height of the Mussel Canopy d_c, Frontal Area Per Volume a, and the Roughness Density λ

Mussel density (mussels m^{-2})	% bed coverage	S (cm)	S/d_c	a (cm^{-1})	λ
0	n/a	n/a	n/a	n/a	n/a
1	0.20	37.02	14.81	0.002	0.01
5	1.02	31.66	12.66	0.002	0.01
10	2.04	17.39	6.96	0.008	0.03
15	3.06	11.83	4.73	0.018	0.06
25	5.11	7.48	2.99	0.045	0.16
35	7.15	4.66	1.87	0.115	0.40
55	11.23	2.23	0.89	0.503	1.76
75	15.32	1.20	0.48	1.745	6.11
100	20.42	0.45	0.18	12.226	42.79

Note. The shaded entries indicate the occurrence of skimming flow for percent bed coverage and S/d_c (Jumars & Nowell, 1984; Knight & Macdonald, 1979; Leonardi et al., 2007; Wolfe & Nickling, 1993) or the occurrence of a dense canopy for λ (Belcher et al., 2003; Nepf, 2012).

For the control experiments with no mussels present, a well-developed boundary layer was present, where the time-averaged and longitudinally averaged flow velocities $\overline{U}_z$ were well described by a logarithmic distribution and distributions of Reynolds shear stress τ_z were nearly linear with height above the bed (Figure 3). Also, for the no-mussel control experiments, shear velocity and the equivalent near-bed Reynolds shear stress τ_w determined from Equation 4 was nearly identical to shear velocity determined from Equation 5 and the maximum Reynolds shear stress τ_{max} determined in Figure 3, respectively, and both values increased with Fr number (Appendix 1). That is, $u_{*w} \approx u_{*\tau}$ and $\tau_w \approx \tau_{max}$ as expected for flat-bed, hydraulically rough turbulent flows (Bennett et al., 1998). In Figure 3 and all subsequent analyses, PIV data were excluded for the 10 mussels m^{-2}, $Fr = 0.12$ experiment due to experimental error. We also note that some near-bed values of τ_z at lower mussel densities were affected by slight imperfections in the height and installation of the bed inserts (Figure 3b).

As mussel density increased, especially at densities above 25 mussels m^{-2}, marked changes in the distribution of longitudinal flow velocity and Reynolds shear stress occurred. Flow velocity just above and below the mussel canopy deviated measurably from the no-mussel control experiments (Figure 3a). Reynolds shear stresses τ_z were reduced within the mussel canopy, and the maximum value of τ_z (τ_{max}) occurred at or just above the mussel canopy top (Figure 3b). Moreover, as mussel density increased, normalized longitudinal flow velocities above the canopy $\overline{U}_O/\overline{U}$ progressively increased and normalized longitudinal flow velocities below the canopy $\overline{U}_I/\overline{U}$ progressively decreased (Figure 4).

Mussel density also impacted the magnitude and distribution of the maximum Reynolds shear stress and the average Reynolds shear stress acting on the mussels. The maximum Reynolds shear stress τ_{max} remained approximately constant for a given Fr number for mussel densities from 0 to 10 mussels m^{-2} (Figure 5a). The parameter τ_{max} became relatively larger as mussel density increased from 15 to 55 mussels m^{-2} and then τ_{max} approached an asymptotic value when mussel density exceeded 55 mussels m^{-2} (τ_{max} became independent of mussel density; Appendix 1). The average Reynolds shear stress stresses acting on the mussels τ_{mussel} are reduced as mussel density increases. Figure 5b displays the variation of τ_{mussel}/τ_{max} as a function of Fr number and mussel density. Values of τ_{mussel}/τ_{max} are also determined for the no mussel condition using Equation 6, and an average value of 0.86 is used here for comparative purposes (actual values are 0.88, 0.87, 0.81, and 0.86 for Fr numbers of 0.12, 0.25, 0.37, and 0.50, respectively). These data show that τ_{mussel}/τ_{max} remains relatively constant up to a mussel density of 15 mussels m^{-2}, and it then decreases measurably at higher densities (although note that the log–log plot obscures scatter in the data for lower mussel densities due to isolated roughness flow). At a mussel density of 100 mussels m^{-2}, τ_{mussel}/τ_{max} is reduced by 38%, 45%, 64%, and 59% for target Fr numbers of 0.15, 0.25, 0.37, and 0.50, respectively, in comparison to the densities less than 15 mussels m^{-2}.

Several roughness indices suggest that the associated changes in near-bed velocity and shear stress as a function of mussel density are indicative of a transition in the flow regime. At lower mussel densities (<15 mussels m^{-2}) where there are few impacts to the longitudinal velocity or shear stress distributions and magnitudes, isolated roughness flow is dominant. The flow regime begins to transition from isolated roughness to wake-interference and skimming flow around 25 mussels m^{-2}. The parameter S/d_c and the percentage of bed coverage of roughness elements exceeds the criteria for skimming flow at 35 and 55 mussels m^{-2}, respectively. Moreover, the nondimensional measure for roughness density λ exceeds the criterion for a dense canopy at 25 mussels m^{-2} (Table 1).

4. Discussion

The results of this study show that over a range of flow conditions, as mussel density increases, the magnitude and distribution of time-averaged values of longitudinal velocity, Reynolds shear stresses near the bed, and maximum Reynolds shear stress are measurably changed. Two distinct flow regimes are observed. At relatively low mussel densities, less than about 25 mussels m^{-2}, the entire water column behaves as a single boundary layer, consistent with hydraulically rough, open channel flow. At a critical mussel density, about 25 mussels m^{-2} given the experimental conditions for this study, a hydrodynamic phenomenon emerges where two distinct flow layers can be demarcated. From the bed to the height of the mussel canopy top, termed the inner flow, longitudinal flow velocities and Reynolds shear stresses τ_z are greatly reduced in comparison to the no-mussel flow condition, and maximum Reynolds shear stress τ_{max} is displaced from the bed to a location at or just above the mussel canopy top (Figures 4 and 5). From the tops of the mussels to the height of the maximum velocity, termed the outer flow, longitudinal flow velocities are increased relative to the no-mussel condition, but maximum Reynolds shear stress remains nearly constant at relatively high mussel densities.

This change in flow regime as a response to mussel density suggests an emergent phenomenon or a hydrodynamic transition that results in skimming flow. Numerous studies have also demonstrated such transitions between flow regimes and regions due to the presence of submerged aquatic vegetation (Ghisalberti, 2009; Nepf & Ghisalberti, 2008) or relatively coarse, immobile sediment (Raus et al., 2019). Moreover, a nondimensional measure of roughness density $\lambda = 0.1$ and an inflection point in the vertical velocity profile at this roughness density can be used to identify skimming flow and to differentiate between sparse and dense canopy limits (Nepf, 2012). In our study, an inflection point is first identified in the vertical velocity profile at 15 mussels m^{-2}, which becomes increasingly apparent as mussel density increases (Figure 3). Accordingly, the nondimensional roughness density λ at 15 mussels m^{-2} is 0.06 and increases to 0.16 at 25 mussels m^{-2}, thus indicating that the density-dependent transition between a sparse and dense canopy occurs between 15 and 25 mussels m^{-2} (Table 1).

Additional criteria for the transition from isolated roughness or wake interference flow regime to a skimming flow regime depend on roughness spacing or density, the vertical location of the maximum Reynolds shear stress, and a reduction in bed roughness. In general, skimming flow occurs when the ratio of the spacing between roughness elements S to the height of the roughness elements (i.e., the height of the mussel canopy top, d_c) is less than about 3 (Knight & Macdonald, 1979; Leonardi et al., 2007; Wolfe & Nickling, 1993). Other studies have suggested that skimming flow also can occur when (1) $S/d_c \approx 1$, (2) more than 8.3% (or 1/12) of the bed surface is covered by roughness elements, and (3) the location of the maximum turbulence intensity rises to the tops of the roughness elements and near-bed shear stress decreases (Jumars & Nowell, 1984). Fully developed skimming can reduce bed roughness, producing quasi-smooth conditions (Knight & Macdonald, 1979; Raupach et al., 1991; Wolfe & Nickling, 1993). Except for the quasi-smooth flow condition, the flow regime transitions to skimming flow when the mussel-covered bed exceeded a density of 25 mussels m^{-2} (Table 1). At these mussel densities and higher and for the mussel sizes used, (1) $S/d_c \lesssim 3$, (2) more than 5% of the bed is covered by mussels (7% at 35 mussels m^{-2} and 11% at 55 mussels m^{-2}), (3) near-bed longitudinal flow velocity is decreased (Figures 3 and 4) and Reynolds shear stresses below the mussel canopy and near the bed are reduced, (4) longitudinal flow velocity above the mussels is increased (Figures 3 and 4), and (5) the maximum Reynolds shear stress moves to the top of the mussel canopy (Figure 3).

In nature, mussel beds are typically composed of multispecies aggregations with multiple size classes and they occur across a wide range of geographic, gradient, and hydraulic scales. In our experiments, we simplified a natural mussel bed by assuming a single size class of mussels within a single species, and all mussels were aligned parallel to the flow with a uniform height of exposure. We also scaled our experiments using Fr number to best match the boundary conditions for a range of baseflow to bank-full flows. To achieve the target Fr number, we varied flow longitudinal velocity and maintained a constant flow depth for all experiments (i.e., 0.15 m). While we understand that this restriction resulted in depth-limited experiments, the range of Fr numbers tested are well aligned to the range of flows the mussels would experience.

Moreover, flow patterns in a flume begin to diverge from natural flow once roughness features occupy more than 35% of the flow depth (Nowell & Jumars, 1987). The model mussels used in this study occupied ~23% of the total flow depth, and therefore, any depth-limitation impacts were considered to be minimal. Accordingly, the complexity of a natural mussel bed will be inherently greater than what we were able to reproduce and the depth over mussel beds will likely be greater than 0.15 m for many flow stages. The hydrodynamic transition observed here would vary across systems based on the composition and arrangement of the mussel fauna present.

Empirical demonstration of this hydrodynamic transition above a mussel-covered bed has significant hydraulic and ecological implications. Relative to the no-mussel control experiment, the average Reynolds shear stress acting on the mussels is reduced by 34% to 64% at a density of 100 mussels m^{-2} for all *Fr* numbers (Figure 5). Such reductions in Reynolds shear stress acting on the mussels means that densely packed mussel beds in rivers would be less likely eroded or dislodged at relatively high flow stages as compared to sparsely populated beds. Similarly, reduced Reynolds shear stresses near the bed would also increase bed stability. It has been suggested that mussel beds may persist for decades at a given river reach because the organisms reside in patches that experience relatively low shear stress even during high flow events (Howard & Cuffey, 2003; Strayer, 1999). Our data, in fact, substantiate this hypothesis, but the physical mechanism is decidedly different. Instead, river beds covered by mussels may experience reduced near-bed shear stresses at all flow stages because of the hydrodynamic emergence of a skimming flow regime caused by the mussels themselves.

The hydraulics of skimming flow with its reduced near-bed shear stresses provide strong evidence for an ecological benefit to riverine mussel beds. The onset of skimming flow due to increased mussel density modifies the local environment such that mussels are less likely to be dislodged by turbulent shear stresses, thus increasing survivorship (i.e., positive density dependency). Relatively dense mussel beds tend to be populated by older mussels (Hastie et al., 2000), which suggest higher survival rates. Mussels older than about 30 years have been found in beds with densities greater than about 5 mussels m^{-2} per species (Haag & Rypel, 2011), and mussel-covered beds commonly found in labile rivers can persist in time for decades (Sansom, Bennett, et al., 2018). Amelioration of stressful habitat conditions via increased densities has been observed in soft sediment marine bivalves, where aggregation prevents dislodgment by waves (Gascoigne et al., 2005) and in intertidal invertebrates where aggregation buffers animals from thermal stress (Bruno et al., 2003). Examples of similar positive density-dependent habitat modification may be more common in communities of sessile aquatic organisms than previously realized and merit further investigation.

The emergence of skimming flows due to mussel aggregation should also lead to increased reproductive and ecological success. Such a positive effect between individual fitness and the number of individuals within a population is referred to as a demographic Allee effect (Kramer et al., 2009; Stephens et al., 1999). Possible aspects include increased fertilization success and filter-feeding efficiency or reduced dislodgment potential. Like many sessile aquatic organisms, mussels are spermcasters. Males release spermatozoa into the water where they must be entrained by the filtering current of a conspecific female. Fertilization success increases with increasing conspecific density (Downing et al., 1993; McLain & Ross, 2005). The fertilization rate in a population of *Margaritifera laevis* in Japan increased with density but only in areas with slow currents (Terui et al., 2015). In areas with higher flow velocities, spermatozoa were displaced downstream regardless of mussel density. Thus, increased mussel density should enhance fertilization success by increasing the proximity of males and females and by creating skimming flow regimes. A skimming flow regime over a mussel bed may allow for spermatozoa to become trapped within the low velocity zones in the inner flow zone below the mussel canopy where females are more likely to receive more gametes and increase reproductive success (Terui et al., 2015) or for increased probability of juvenile mussels establishing in suitable habitat in low velocity zones in the inner flow zone below the mussel canopy.

A possible drawback to the increased roughness created by the mussels is the potential for enhanced sediment suspension or deposition. Previous studies with submerged vegetation have observed concentrated ejection and sweep events at the canopy top (Ghisalberti & Nepf, 2008; Tinoco & Coco, 2016). Moreover, in experiments with dense arrays of submerged, rigid cylinders and marine bivalves, even though flow

speed was significantly reduced within the canopy, an increase in sediment suspension was observed due to intermittent turbulent ejections and patch-scale turbulence (Tinoco & Coco, 2016; Widdows et al., 2009). Sediment suspension caused by mussel roughness was also found to suspend microphytobenthos, thus further elucidating that self-organized mussel communities enhance food provision through sediment suspension that offsets the filtering of phytoplankton above the mussel canopy (Widdows et al., 2009). It should also be noted that sediment suspension due to dense canopies was observed for sand/muddy beds (Tinoco & Coco, 2016; Widdows et al., 2009). In river systems with coarser substrate, dense mussel canopies might actually serve to armor the bed (Johnson & Brown, 2000; Zimmerman & de Szalay, 2007), or mussels may self-align so that only phytoplankton rich sediments are suspended while the remaining substrate serves to aid in anchoring individual mussels, but such hypotheses warrant further investigation.

The results of this study show that there is a density-dependent interaction between mussels and flow, and above a critical density, marked changes in the flow regime occur that enhance the long-term persistence of mussels. A better understanding of the mussel density at which this occurs would greatly improve conservation efforts. Establishing minimum viable population sizes for threatened mussel species is important for conservation, but no criteria have been estimated for many mussel species (Mosley et al., 2014). The hydrodynamic transition observed in our study, beginning at 25 mussels m^{-2} and quantified by several roughness indices (i.e., S/k, percent bed coverage, and roughness density), may be indicative of a potential minimum viable population target (Shaffer, 1981; Traill et al., 2007) for both ecological and hydrodynamic benefits. While similar hydrodynamic transitions will likely vary across systems and be dependent on species and mussel burrow position, the results of this study suggest that critical thresholds of mussel density exist at which mussels are capable of reducing near-bed shear stresses that would increase long-term persistence. In fact, a recent freshwater mussel restoration effort proposed a target restoration density of 25 mussels m^{-2} for Pendleton Island on the Clinch River, VA (Jones et al., 2018). Although higher densities could be supported in this waterway, a historical baseline density of 25 mussels m^{-2} was proposed for assessing the success and resiliency of these conservation activities. This historical baseline density further suggests that Allee effects or minimum viable population sizes exist for freshwater mussels, but these density-dependent interactions need to be further explored in the context of ecological and hydrodynamic benefits.

5. Conclusions

For the given flow conditions and mussel sizes used herein, we demonstrated that freshwater mussel densities in excess of 25 mussels m^{-2} on a gravel-bedded river channel create an emergent hydrodynamic phenomenon known as skimming flow. This skimming flow regime increases time-averaged longitudinal flow velocity above the mussel canopy, decreases time-averaged longitudinal flow velocity within the mussel canopy, and reduces the time-averaged near-bed turbulent shear stresses acting to dislodge the organisms. The ability of this mussel-flow interaction to modify the hydrodynamic habitat of stream ecosystems has important ecological and conservation implications. Skimming flows over mussel covered beds, interpreted here as a potential Allee effect, enhance habitat complexity by creating distinct regions of demarcated flow zones, contribute to a reduction in sediment erosion by displacing the maximum shear stress off the bed and higher into the water column, and may enhance the ecological success of mussels. Based on these results and from other studies quantifying mussel burrow position and diversity within mussel communities (Allen & Vaughn, 2009; Sansom, 2018), multispecies aggregates of mussels are likely able to create a flow environment that decreases the turbulent shear stresses acting to dislodge the organisms. Determining this threshold density across systems and species can be used to establish a minimum viable population for mussels in gravel-bedded channels. Such information is critical to future conservation and management strategies that aim to maintain healthy mussel beds or reintroduce mussel populations.

Appendix A

Water Resources Research

10.1029/2019WR026252

Table A1
PIV Experimental Data and Statistics

							Data calculated from the Kármán-Prandtl "law of the wall"				Data calculated from the maximum Reynolds stress				
Mussel density (mussels m^{-2})	Target Fr #	Maximum $\overline{U}_z$ (m/s)	Height of maximum $\overline{U}_z$ (m)	$\overline{U}$ (m/s)	$\overline{U}_I$ (m/s)	$\overline{U}_O$ (m/s)	u_{*w} (m/s)	u_{*w} SE (m/s)	τ_w (Pa)	τ_w SE (Pa)	$u_{*\tau}$ (m/s)	$u_{*\tau}$ SE (m/s)	τ_{max} (Pa)	τ_{max} SE (Pa)	Height of τ_{max} (m)
0	0.12	0.16	0.130	0.14	-	0.14	0.01	4.2E-06	0.07	7.3E-05	0.01	7.2E-05	0.12	1.6E-03	0.015
0	0.25	0.32	0.126	0.27	-	0.27	0.02	9.2E-05	0.38	3.6E-03	0.02	8.8E-05	0.45	3.8E-03	0.019
0	0.37	0.46	0.134	0.37	-	0.37	0.03	4.2E-04	0.86	2.5E-02	0.03	7.5E-05	0.99	4.8E-03	0.048
0	0.50	0.66	0.130	0.53	-	0.53	0.04	5.3E-04	1.87	4.5E-02	0.04	3.8E-04	1.88	3.3E-02	0.037
1	0.12	0.16	0.131	0.14	0.10	0.15	-	-	-	-	0.01	2.8E-04	0.10	5.8E-03	0.015
1	0.25	0.33	0.123	0.27	0.21	0.30	-	-	-	-	0.02	1.6E-04	0.41	6.3E-03	0.007
1	0.37	0.47	0.127	0.39	0.29	0.42	-	-	-	-	0.03	2.1E-04	0.88	1.3E-02	0.015
1	0.50	0.66	0.131	0.55	0.40	0.61	-	-	-	-	0.04	2.3E-04	1.77	1.9E-02	0.015
5	0.12	0.17	0.126	0.14	0.10	0.15	-	-	-	-	0.01	1.0E-04	0.10	2.1E-03	0.011
5	0.25	0.33	0.126	0.27	0.21	0.30	-	-	-	-	0.02	1.8E-04	0.39	7.0E-03	0.011
5	0.37	0.46	0.126	0.37	0.27	0.41	-	-	-	-	0.03	1.5E-04	0.83	8.7E-03	0.045
5	0.50	0.66	0.126	0.54	0.37	0.61	-	-	-	-	0.04	1.7E-04	1.64	1.4E-02	0.015
10	0.12	-	-	-	-	-	-	-	-	-	-	-	-	-	-
10	0.25	0.33	0.127	0.27	0.20	0.30	-	-	-	-	0.02	6.5E-04	0.59	3.2E-02	0.011
10	0.37	0.48	0.127	0.39	0.27	0.43	-	-	-	-	0.04	6.0E-04	1.32	4.4E-02	0.011
10	0.50	0.66	0.134	0.53	0.35	0.59	-	-	-	-	0.05	7.9E-04	2.69	8.3E-02	0.011
15	0.12	0.16	0.127	0.13	0.09	0.15	-	-	-	-	0.01	6.3E-04	0.14	1.5E-02	0.004
15	0.25	0.36	0.123	0.29	0.20	0.33	-	-	-	-	0.03	8.4E-04	0.67	4.4E-02	0.019
15	0.37	0.48	0.127	0.40	0.28	0.45	-	-	-	-	0.04	9.2E-04	1.34	6.8E-02	0.015
15	0.50	0.67	0.134	0.53	0.33	0.60	-	-	-	-	0.05	7.6E-04	2.13	7.1E-02	0.015
25	0.12	0.17	0.131	0.13	0.09	0.15	-	-	-	-	0.01	2.0E-04	0.14	4.9E-03	0.019
25	0.25	0.35	0.131	0.28	0.18	0.32	-	-	-	-	0.02	7.6E-04	0.54	3.6E-02	0.011
25	0.37	0.50	0.127	0.39	0.25	0.45	-	-	-	-	0.04	6.7E-04	1.40	5.0E-02	0.019
25	0.50	0.73	0.135	0.54	0.28	0.64	-	-	-	-	0.05	1.5E-03	2.85	1.6E-01	0.037
35	0.12	0.16	0.130	0.13	0.08	0.15	-	-	-	-	0.01	1.8E-04	0.16	4.5E-03	0.026
35	0.25	0.35	0.134	0.26	0.13	0.31	-	-	-	-	0.03	7.5E-04	0.71	4.1E-02	0.037
35	0.37	0.51	0.130	0.39	0.24	0.45	-	-	-	-	0.04	2.9E-04	1.53	2.3E-02	0.026
35	0.50	0.69	0.130	0.53	0.30	0.61	-	-	-	-	0.05	8.3E-04	2.77	8.8E-02	0.033
55	0.12	0.18	0.134	0.13	0.07	0.15	-	-	-	-	0.01	4.6E-05	0.19	1.3E-03	0.041
55	0.25	0.36	0.134	0.26	0.13	0.30	-	-	-	-	0.03	1.3E-04	0.81	7.6E-03	0.041
55	0.37	0.51	0.126	0.39	0.24	0.45	-	-	-	-	0.04	1.6E-04	1.77	1.4E-02	0.033
55	0.50	0.70	0.130	0.52	0.30	0.61	-	-	-	-	0.06	2.8E-04	3.48	3.3E-02	0.037
75	0.12	0.17	0.127	0.12	0.06	0.14	-	-	-	-	0.01	2.1E-04	0.20	5.9E-03	0.034
75	0.25	0.35	0.124	0.24	0.14	0.29	-	-	-	-	0.02	2.4E-04	0.61	1.2E-02	0.034
75	0.37	0.51	0.127	0.36	0.20	0.43	-	-	-	-	0.04	1.0E-04	1.64	8.1E-03	0.041
75	0.50	0.71	0.135	0.48	0.24	0.57	-	-	-	-	0.05	1.4E-04	3.01	1.5E-02	0.052
100	0.12	0.17	0.136	0.12	0.06	0.14	-	-	-	-	0.01	9.3E-05	0.20	2.6E-03	0.045
100	0.25	0.34	0.132	0.23	0.10	0.28	-	-	-	-	0.03	2.6E-04	0.80	1.5E-02	0.045
100	0.37	0.50	0.127	0.34	0.17	0.42	-	-	-	-	0.04	3.8E-04	1.67	3.2E-02	0.049
100	0.50	0.70	0.131	0.47	0.21	0.58	-	-	-	-	0.06	6.3E-04	3.55	7.6E-02	0.045

Note. The Kármán-Prandtl "law of the wall" statistics were only calculated for the no-mussel control. PIV data were excluded for the 10 mussels m^{-2}, $Fr = 0.12$ experiment due to experimental error.

Acknowledgments

This research was supported by the National Science Foundation grant EAR 1659909. We thank Dr. Elizabeth Kapral and the Erie County Medical Center, Department of Oral Oncology and Maxiillofacial Prosthetic, who provided access and assistance in using the Cone Beam Computed Tomography scanner to obtain a three-dimensional scan of the freshwater mussel shell, and Kevin Cullinan and Tomas Gruenauer, who assisted in manufacturing the model mussels used in this study. We thank three anonymous reviewers, who provided helpful comments that improved this manuscript. Data used in this paper are available for download from the following data repository (https://www.hydroshare.org/resource/f54f6472f3cf4e3fb9e7b54ccd529a7f).

References

Allan, J. D., & Castillo, M. M. (2007). *Stream ecology: Structure and function of running waters* (2nd ed.). Netherlands: Springer. Retrieved from https://www.springer.com/gp/book/9781402055829

Allen, D. C., Cardinale, B. J., & Wynn-Thompson, T. (2014). Toward a better integration of ecological principles into ecogeoscience research. *Bioscience*, *64*(5), 444–454. https://doi.org/10.1093/biosci/biu046

Allen, D. C., & Vaughn, C. C. (2009). Burrowing behavior of freshwater mussels in experimentally manipulated communities. *Journal of the North American Benthological Society*, *28*(1), 93–100. https://doi.org/10.1899/07-170.1

Allen, D. C., & Vaughn, C. C. (2010). Complex hydraulic and substrate variables limit freshwater mussel species richness and abundance. *Journal of the North American Benthological Society*, *29*(2), 383–394. https://doi.org/10.1899/09-024.1

Atkinson, C. L., & Vaughn, C. C. (2015). Biogeochemical hotspots: Temporal and spatial scaling of the impact of freshwater mussels on ecosystem function. *Freshwater Biology*, *60*(3), 563–574. https://doi.org/10.1111/fwb.12498

Atkinson, C. L., Vaughn, C. C., Forshay, K. J., & Cooper, J. T. (2013). Aggregated filter-feeding consumers alter nutrient limitation: Consequences for ecosystem and community dynamics. *Ecology*, *94*(6), 1359–1369. https://doi.org/10.1890/12-1531.1

Belcher, S. E., Jerram, N., & Hunt, J. C. R. (2003). Adjustment of a turbulent boundary layer to a canopy of roughness elements. *Journal of Fluid Mechanics*, *488*, 369–398. https://doi.org/10.1017/S0022112003005019

Bennett, S. J., Bridge, J. S., & Best, J. L. (1998). Fluid and sediment dynamics of upper stage plane beds. *Journal of Geophysical Research*, *103*(C1), 1239–1274. https://doi.org/10.1029/97JC02764

Bruno, J. F., Stachowicz, J. J., & Bertness, M. D. (2003). Inclusion of facilitation into ecological theory. *Trends in Ecology & Evolution*, *18*(3), 119–125. https://doi.org/10.1016/S0169-5347(02)00045-9

Cardinale, B. J., Gelmann, E. R., & Palmer, M. A. (2004). Net spinning caddisflies as stream ecosystem engineers: The influence of hydropsyche on benthic substrate stability. *Functional Ecology*, *18*(3), 381–387. https://doi.org/10.1111/j.0269-8463.2004.00865.x

Chow, V. T. (1959). *Open-channel hydraulics*. New York, NY: McGraw-Hill Companies.

Constantinescu, G., Miyawaki, S., & Liao, Q. (2013). Flow and turbulence structure past a cluster of freshwater mussels. *Journal of Hydraulic Engineering*, *139*(4), 347–358. https://doi.org/10.1061/(ASCE)HY.1943-7900.0000692

Davis, J. A. (1986). Boundary layers, flow microenvironments and stream benthos. In P. De Deckker, & W. D. Williams (Eds.), *Limnology in Australia* (pp. 293–312). Dordrecht: Springer Netherlands. https://doi.org/10.1007/978-94-009-4820-4_18

Davis, J. A., & Barmuta, L. A. (1989). An ecologically useful classification of mean and near-bed flows in streams and rivers. *Freshwater Biology*, *21*(2), 271–282. https://doi.org/10.1111/j.1365-2427.1989.tb01365.x

Downing, J. A., Rochon, Y., Pérusse, M., & Harvey, H. (1993). Spatial aggregation, body size, and reproductive success in the freshwater mussel Elliptio complanata. *Journal of the North American Benthological Society*, *12*(2), 148–156. https://doi.org/10.2307/1467344

Gangloff, M. M., & Feminella, J. W. (2006). Stream channel geomorphology influences mussel abundance in southern Appalachian streams, U.S.A. *Freshwater Biology*, *52*, 64–74. https://doi.org/10.1111/j.1365-2427.2006.01673.x

Gascoigne, J. C., Beadman, H. A., Saurel, C., & Kaiser, M. J. (2005). Density dependence, spatial scale and patterning in sessile biota. *Oecologia*, *145*(3), 371–381. https://doi.org/10.1007/s00442-005-0137-x

Ghisalberti, M. (2009). Obstructed shear flows: Similarities across systems and scales. *Journal of Fluid Mechanics*, *641*, 51–61. https://doi.org/10.1017/S0022112009992175

Ghisalberti, M., & Nepf, H. (2008). Shallow flows over a permeable medium: The hydrodynamics of submerged aquatic canopies. *Transport in Porous Media*, *78*(2), 309–326. https://doi.org/10.1007/s11242-008-9305-x

Goring, D. G., & Nikora, V. I. (2002). Despiking acoustic doppler velocimeter data. *Journal of Hydraulic Engineering*, *128*(1), 117–126. https://doi.org/10.1061/(ASCE)0733-9429(2002)128:1(117)

Gutiérrez, J. L., Jones, C. G., Strayer, D. L., & Iribarne, O. O. (2003). Mollusks as ecosystem engineers: The role of shell production in aquatic habitats. *Oikos*, *101*(1), 79–90. https://doi.org/10.1034/j.1600-0706.2003.12322.x

Haag, W. R. (2012). *North American freshwater mussels: natural history, ecology, and conservation*. Cambridge, UK: Cambridge University Press.

Haag, W. R., & Rypel, A. L. (2011). Growth and longevity in freshwater mussels: Evolutionary and conservation implications. *Biological Reviews*, *86*(1), 225–247. https://doi.org/10.1111/j.1469-185X.2010.00146.x

Hardison, B. S., & Layzer, J. B. (2001). Relations between complex hydraulics and the localized distribution of mussels in three regulated rivers. *Regulated Rivers: Research & Management*, *17*(1), 77–84. https://doi.org/10.1002/1099-1646(200101/02)17:1<77::AID-RRR604>3.0.CO;2-S

Hastie, L. C., Young, M. R., Boon, P. J., Cosgrove, P. J., & Henninger, B. (2000). Sizes, densities and age structures of Scottish *Margaritifera margaritifera* (L.) populations. *Aquatic Conservation: Marine and Freshwater Ecosystems*, *10*(4), 229–247. https://doi.org/10.1002/1099-0755(200007/08)10:4<229::AID-AQC409>3.0.CO;2-3

Hopper, G. W., DuBose, T. P., Gido, K. B., & Vaughn, C. C. (2019). Freshwater mussels alter fish distributions through habitat modifications at fine spatial scales. *Freshwater Science*, *38*(4), 702–712. https://doi.org/10.1086/705666

Howard, J. K., & Cuffey, K. M. (2003). Freshwater mussels in a California north coast range river: Occurrence, distribution, and controls. *Journal of the North American Benthological Society*, *22*(1), 63–77. https://doi.org/10.2307/1467978

Johnson, P. D., & Brown, K. M. (2000). The importance of microhabitat factors and habitat stability to the threatened Louisiana pearl shell, *Margaritifera hembeli* (Conrad). *Canadian Journal of Zoology*, *78*(2), 271–277. https://doi.org/10.1139/z99-196

Jones, C. G., Lawton, J. H., & Shachak, M. (1994). Organisms as ecosystem engineers. *Oikos*, *69*(3), 373–386. https://doi.org/10.2307/3545850

Jones, J., Lane, T., Ostby, B., Beaty, B., Ahlstedt, S., Butler, R., et al. (2018). Collapse of the Pendleton Island mussel fauna in the Clinch River, Virginia: Setting baseline conditions to guide recovery and restoration. *Freshwater Mollusk Biology and Conservation*, *21*(2), 36–57. https://doi.org/10.31931/fmbc.v21i2.2018.36-56

Jones, J. I., Collins, A. L., Naden, P. S., & Sear, D. A. (2012). The relationship between fine sediment and macrophytes in rivers. *River Research and Applications*, *28*(7), 1006–1018. https://doi.org/10.1002/rra.1486

Jumars, P. A., & Nowell, A. R. M. (1984). Fluid and sediment dynamic effects on marine benthic community structure. *Integrative and Comparative Biology*, *24*(1), 45–55. https://doi.org/10.1093/icb/24.1.45

Knight, D. W., & Macdonald, J. A. (1979). Hydraulic resistance of artificial strip roughness. *Journal of the Hydraulics Division*, *105*(6), 675–690.

Kramer, A. M., Dennis, B., Liebhold, A. M., & Drake, J. M. (2009). The evidence for Allee effects. *Population Ecology*, *51*(3), 341–354. https://doi.org/10.1007/s10144-009-0152-6

Kumar, S. S., Kozarek, J., Hornbach, D., Hondzo, M., & Hong, J. (2019). Experimental investigation of turbulent flow over live mussels. *Environmental Fluid Mechanics*, *19*(6), 1417–1430. https://doi.org/10.1007/s10652-019-09664-2

Layzer, J. B., & Madison, L. M. (1995). Microhabitat use by freshwater mussels and recommendations for determining their instream flow needs. *Regulated Rivers: Research & Management*, *10*(2–4), 329–345. https://doi.org/10.1002/rrr.3450100225

Leonardi, S., Orlandi, P., & Antonia, R. A. (2007). Properties of d- and k-type roughness in a turbulent channel flow. *Physics of Fluids*, *19*(12), 125101. https://doi.org/10.1063/1.2821908

Lohrer, A. M., Thrush, S. F., & Gibbs, M. M. (2004). Bioturbators enhance ecosystem function through complex biogeochemical interactions. *Nature*, *431*(7012), 1092–1095. https://doi.org/10.1038/nature03042

McLain, D. C., & Ross, M. R. (2005). Reproduction based on local patch size of *Alasmidonta heterodon* and dispersal by its darter host in the Mill River, Massachusetts, USA. *Journal of the North American Benthological Society*, *24*(1), 139–147. https://doi.org/10.1899/0887-3593(2005)024<0139:RBOLPS>2.0.CO;2

Monismith, S. G., Koseff, J. R., Thompson, J. K., O'Riordan, C. A., & Nepf, H. M. (1990). A study of model bivalve siphonal currents. *Limnology and Oceanography*, *35*(3), 680–696. https://doi.org/10.4319/lo.1990.35.3.0680

Morales, Y., Weber, L. J., Mynett, A. E., & Newton, T. J. (2006a). Effects of substrate and hydrodynamic conditions on the formation of mussel beds in a large river. *Journal of the North American Benthological Society*, *25*(3), 664–676. https://doi.org/10.1899/0887-3593(2006)25[664:EOSAHC]2.0.CO;2

Morales, Y., Weber, L. J., Mynett, A. E., & Newton, T. J. (2006b). Mussel dynamics model: A hydroinformatics tool for analyzing the effects of different stressors on the dynamics of freshwater mussel communities. *Ecological Modelling*, *197*(3–4), 448–460. https://doi.org/10.1016/j.ecolmodel.2006.03.018

Morris, H. M. (1955). Flow in rough conduits. *Transactions of the American Society of Civil Engineers*, *120*(1), 373–398.

Mosley, T. L., Haag, W. R., & Stoeckel, J. A. (2014). Egg fertilisation in a freshwater mussel: Effects of distance, flow and male density. *Freshwater Biology*, *59*(10), 2137–2149. https://doi.org/10.1111/fwb.12417

Murphy, E., Ghisalberti, M., & Nepf, H. (2007). Model and laboratory study of dispersion in flows with submerged vegetation. *Water Resources Research*, *43*, W05438. https://doi.org/10.1029/2006WR005229

Nakano, D., Yamamoto, M., & Okino, T. (2005). Ecosystem engineering by larvae of net-spinning stream caddisflies creates a habitat on the upper surface of stones for mayfly nymphs with a low resistance to flows. *Freshwater Biology*, *50*(9), 1492–1498. https://doi.org/10.1111/j.1365-2427.2005.01421.x

Nepf, H. M. (2012). Hydrodynamics of vegetated channels. *Journal of Hydraulic Research*, *50*(3), 262–279. https://doi.org/10.1080/00221686.2012.696559

Nepf, H. M., & Ghisalberti, M. (2008). Flow and transport in channels with submerged vegetation. *Acta Geophysica*, *56*(3), 753–777. https://doi.org/10.2478/s11600-008-0017-y

Nepf, H. M., & Vivoni, E. R. (2000). Flow structure in depth-limited, vegetated flow. *Journal of Geophysical Research*, *105*(C12), 28,547–28,557. https://doi.org/10.1029/2000JC900145

Nikora, V. (2010). Hydrodynamics of aquatic ecosystems: An interface between ecology, biomechanics and environmental fluid mechanics. *River Research and Applications*, *26*(4), 367–384. https://doi.org/10.1002/rra.1291

Nowell, A. R. M., & Jumars, P. A. (1987). Flumes: Theoretical and experimental considerations for simulation of benthic environments. *Oceanography and Marine Biology: An Annual Review*, *27*, 91–112.

O'Riordan, C. A., Monismith, S. G., & Koseff, J. R. (1993). A study of concentration boundary-layer formation over a bed of model bivalves. *Limnology and Oceanography*, *38*(8), 1712–1729. https://doi.org/10.4319/lo.1993.38.8.1712

Parmalee, P. W., & Bogan, A. E. (1998). *The freshwater mussels of Tennessee*. Knoxville, Tenn: University of Tennessee Press.

Perry, A. E., Schofield, W. H., & Joubert, P. N. (1969). Rough wall turbulent boundary layers. *Journal of Fluid Mechanics*, *37*(2), 383–413. https://doi.org/10.1017/S0022112069000619

Raupach, M. R., Antonia, R. A., & Rajagopalan, S. (1991). Rough-wall turbulent boundary layers. *Applied Mechanics Reviews*, *44*(1), 1–25. https://doi.org/10.1115/1.3119492

Raus, D., Moulin, F. Y., & Eiff, O. (2019). The impact of coarse-grain protrusion on near-bed hydrodynamics. *Journal of Geophysical Research: Earth Surface*, *124*, 1854–1877. https://doi.org/10.1029/2018JF004751

Sansom, B. J. (2018). Freshwater mussels as ecosystem engineers: Modulation of near bed hydrodynamics through mussel-flow interactions (Dissertation). SUNY University at Buffalo, Buffalo, NY.

Sansom, B. J., Atkinson, J. F., & Bennett, S. J. (2018). Modulation of near-bed hydrodynamics by freshwater mussels in an experimental channel. *Hydrobiologia*, *810*(1), 449–463. https://doi.org/10.1007/s10750-017-3172-9

Sansom, B. J., Bennett, S. J., Atkinson, J. F., & Vaughn, C. C. (2018). Long-term persistence of freshwater mussel beds in labile river channels. *Freshwater Biology*, *63*(11), 1469–1481. https://doi.org/10.1111/fwb.13175

Shaffer, M. L. (1981). Minimum population sizes for species conservation. *Bioscience*, *31*(2), 131–134. https://doi.org/10.2307/1308256

Spooner, D. E., Vaughn, C. C., & Galbraith, H. S. (2012). Species traits and environmental conditions govern the relationship between biodiversity effects across trophic levels. *Oecologia*, *168*(2), 533–548. https://doi.org/10.1007/s00442-011-2110-1

Statzner, B., Gore, J. A., & Resh, V. H. (1988). Hydraulic stream ecology: Observed patterns and potential applications. *Journal of the North American Benthological Society*, *7*(4), 307–360. https://doi.org/10.2307/1467296

Stephens, P. A., Sutherland, W. J., & Freckleton, R. P. (1999). What is the Allee effect? *Oikos*, *87*(1), 185–190. https://doi.org/10.2307/3547011

Strayer, D. L. (1999). Use of flow refuges by unionid mussels in rivers. *Journal of the North American Benthological Society*, *18*(4), 468–476. https://doi.org/10.2307/1468379

Strayer, D. L. (2008). *Freshwater mussel ecology: A multifactor approach to distribution and abundance*. Berkeley, USA: University of California Press.

Strayer, D. L., Hunter, D. C., Smith, L. C., & Borg, C. K. (1994). Distribution, abundance, and roles of freshwater clams (Bivalvia, Unionidae) in the freshwater tidal Hudson River. *Freshwater Biology*, *31*(2), 239–248. https://doi.org/10.1111/j.1365-2427.1994.tb00858.x

Terui, A., Miyazaki, Y., Yoshioka, A., & Matsuzaki, S. S. (2015). A cryptic Allee effect: Spatial contexts mask an existing fitness–density relationship. *Royal Society Open Science*, *2*, 150034. https://doi.org/10.1098/rsos.150034

Tinoco, R. O., & Coco, G. (2016). A laboratory study on sediment resuspension within arrays of rigid cylinders. *Advances in Water Resources*, *92*, 1–9. https://doi.org/10.1016/j.advwatres.2016.04.003

Traill, L. W., Bradshaw, C. J. A., & Brook, B. W. (2007). Minimum viable population size: A meta-analysis of 30 years of published estimates. *Biological Conservation*, *139*(1), 159–166. https://doi.org/10.1016/j.biocon.2007.06.011

von Karman, T. H. (1931). Mechanical similitude and turbulence (Technical Memorandum 611). National Advisory Committee for Aeronautics.

Widdows, J., Pope, N. D., Brinsley, M. D., Gascoigne, J., & Kaiser, M. J. (2009). Influence of self-organised structures on near-bed hydrodynamics and sediment dynamics within a mussel (Mytilus edulis) bed in the Menai Strait. *Journal of Experimental Marine Biology and Ecology*, *379*(1), 92–100. https://doi.org/10.1016/j.jembe.2009.08.017

Wolfe, S. A., & Nickling, W. G. (1993). The protective role of sparse vegetation in wind erosion. *Progress in Physical Geography: Earth and Environment*, *17*(1), 50–68. https://doi.org/10.1177/030913339301700104

Wooding, R. A., Bradley, E. F., & Marshall, J. K. (1973). Drag due to regular arrays of roughness elements of varying geometry. *Boundary-Layer Meteorology*, *5*(3), 285–308. https://doi.org/10.1007/BF00155238

Zimmerman, G. F., & de Szalay, F. A. (2007). Influence of unionid mussels (Mollusca: Unionidae) on sediment stability: An artificial stream study. *Fundamental and Applied Limnology*, *168*(4), 299–306. https://doi.org/10.1127/1863-9135/2007/0168-0299